Journal of Oceanography
https://doi.org/10.1007/s10872-025-00780-w

ORIGINAL ARTICLE

Sediment resuspension and its occurring conditions in the Soya warm current region observed from ADCP backscatter strength

Mizuki Kuga[1,5] · Kay I. Ohshima[1,2,3] · Yasushi Fukamachi[3] · Masato Ito[4] · Jun Nishioka[2,3]

Received: 25 April 2024 / Revised: 25 August 2025 / Accepted: 8 October 2025

Abstract

One of the major sources of iron supply to the Okhotsk Sea and the Oyashio region, which both have high biological productivity, is thought to be regions of the East Sakhalin Current and its upstream, originating from the Amur River. This study suggests that the Soya Warm Current (SWC) region could also be a possible source of iron via resuspension of bottom sediments. We derived the volume backscatter strength from acoustic Doppler current profilers (ADCP) data that had previously been collected in the SWC region. The backscatter strength data indicate that prominent sediment resuspension occurs in both the upstream and downstream regions of the SWC when the bottom current exceeding 0.5 m/s continues to some extent. In the upstream region, strong current events that induced the sediment resuspension occurred through the SWC intensification caused by the increase in sea-level difference across the Soya Strait excited by the southerly winds. Such events frequently occur from September to December, because of frequent passages of cyclone. By contrast, in the downstream region, sediment resuspension occurred due to the strong northerly winds via the current increase caused by the coastal trapped waves over the shelf in winter. The sediment resuspension in the downstream region was also supported by direct observations of high turbidity near the bottom. High iron concentrations in the coastal Oyashio water possibly originate from the SWC water. The occurrence of the resuspension during the sea ice season suggests the potential local incorporation of sediment into sea ice.

Keywords Sediment resuspension · ADCP · Backscatter strength · Soya warm current · Coastal-trapped wave

1 Introduction

The Sea of Okhotsk and the Oyashio region are characterized by high biological productivity, which is partly due to the water supply having a high concentration of iron, an essential micro-nutrient for phytoplankton (e.g. Nishioka et al. 2021). This iron-rich water is considered to originate from two sources: the Okhotsk Sea Intermediate Water (OSIW) and the sea ice melt water in the southwestern Okhotsk Sea.

The iron in the OSIW is considered to originate from the Amur River. Once the iron from the river accumulates over the northwestern continental shelf or the east Sakhalin shelf, it then enters into dense shelf water (DSW: 26.8–27.0σ_θ) through sediment resuspension assisted by the strong tidal currents (Nakatsuka et al. 2004). The iron is incorporated into the OSIW through DSW (Nishioka et al. 2014), and it is subsequently transported into the upper layer via strong tidal mixing in the Kuril Straits (Nishioka et al. 2013). Finally, it extends to the Oyashio region (Nishioka et al. 2011).

Regarding iron from the sea ice melt water in the southwestern Okhotsk Sea, Kanna et al. (2014; 2018) made direct observations in the southern part of the sea and showed that the sea ice contains significantly higher particulate iron concentrations than the surface water. They also showed

✉ Mizuki Kuga
kuga_mizuki53@fra.go.jp

1 Institute of Low Temperature Science, Hokkaido University, Sapporo, Hokkaido, Japan

2 Pan-Okhotsk Research Center, Institute of Low Temperature Science, Hokkaido University, Sapporo, Hokkaido, Japan

3 Arctic Research Center, Hokkaido University, Sapporo, Hokkaido, Japan

4 National Institute of Polar Research, Tachikawa, Tokyo, Japan

5 Present address: Japan Fisheries Research and Education Agency, Fisheries Resources Institute, Nagasaki, Nagasaki, Japan

Published online: 17 November 2025

that iron released by the sea ice melt water contributes to primary biological production. In the Kuril Basin, areas affected by the sea ice melt exhibit higher net community production (NCP) during the prominent spring bloom (Kishi et al. 2021). Particle-tracking experiments on sea ice floes suggested that the sea ice melting in the high NCP area originates from the coastal polynyas off Sakhalin (Kuga et al. 2023, 2024). Kanna et al. (2014) proposed that the source of particulate iron contained in the sea ice in the southern part of the sea originates from the bottom sediments. Regarding the mechanism for incorporation of sediments into sea ice, Ito et al. (2017; 2021) suggested the interaction between sedimentary particles and frazil ice resulting from the simultaneous occurrence, called as suspension freezing and the incorporation of bottom sediment by frazil ice that reaches the bottom due to the winter convection.

For both sources of iron, the origin is the sediments over the northwestern and east Sakhalin shelves, upstream of the East Sakhalin Current (ESC). So far, it has been believed that the northwestern and east Sakhalin shelves associated with the ESC are the main source of iron. However, very recently, a snapshot observation showed high iron concentrations near the bottom in the Soya Warm Current (SWC) region, preliminarily reported by Imai et al. (2024). There was also a snapshot observation of high turbidity water in the bottom layer in the SWC region (Wadaka et al. 2009). Although there have been only two snapshot observations of high iron or turbidity in the SWC region, there is a possibility that not only the upstream of the ESC but also the SWC region could be a source of iron. According to the backward tracking simulations of sea ice sampled in the southwestern part of the sea, sea ice originating from the area near the Hokkaido coast could also have high iron concentrations (Kuga et al. 2024), which suggests the possibility of local entrainment of sediments into sea ice. However, there have been no specific observations of the sediment resuspension in the SWC region. Does sediment resuspension occur actively in this region? If this is the case, when does the resuspension occur and what is the condition of its occurrence? Does the resuspension occurrence depend on the season? To clarify them, long-term continuous observation that could detect sediment resuspension is needed.

Ito et al. (2017; 2019) showed that backscatter strength information obtained from moored acoustic Doppler current profilers (ADCPs) could be used to detect sediment resuspension. Then, on the basis of the moored ADCP data, they reported that a strong current with a typical speed of exceeding 50 cm/s near the seafloor causes significant sediment resuspension in the ESC region (Ito et al. 2017) and the coastal Chukchi Sea (Ito et al. 2019).

The SWC is a coastal current along the Hokkaido coast that carries warm saline water from the Japan Sea, and the current axis is located between 20 and 30 km from the coast (Ebuchi et al. 2006; Ohshima et al. 2017). The vertical structure of the current has a baroclinic component, with larger surface velocities exceeding 90 cm/s in summer and larger bottom velocities in winter (Fukamachi et al. 2008; Ohshima et al. 2017). In the SWC region, long-term moored ADCP observations were carried out near the Soya Strait (Fukamachi et al. 2008, 2010) and in the downstream region (Fukamachi et al. 2003, 2006). The current speed near the seafloor often exceeds 50 cm/s (Fukamachi et al. 2008), which could provide a condition for the sediment resuspension, although it may also depend on the geology of the seafloor. These studies treated only the current velocity from the ADCP, and the backscatter strength information from the ADCP has not been used at all.

The primary objective of this study is to clarify whether the sediment resuspension occurs in the SWC region by deriving the backscatter strength data from these accumulated ADCP data. As will be shown, the backscatter strength data clearly indicate that sediment resuspension occurs when the bottom current is strong. Therefore, we also investigate the condition of the strong current that could induce the resuspension to examine the seasonal variations of resuspension, which could provide important information for the iron supply from the SWC region. Furthermore, we made the direct observations of the turbidity in the SWC region to obtain the evidence of the sediment resuspension.

This paper is organized as follows. Section 2 describes the observations and data with the derivation of the ADCP backscatter strength data. Section 3 shows that the prominent resuspension of sediments often occurs in autumn upstream of the SWC, detected by the ADCP backscatter strength data. The conditions leading to occurrence of sediment resuspension and its seasonal variations are also examined. Section 4 describes the sediment resuspension in the downstream region of the SWC, using the ADCP data and turbidity measurements. Section 5 provides summary and discussion.

2 Data and methods

2.1 ADCP observations

We used ADCP (WH-Sentinel 300 kHz manufactured by RD Instruments) data observed at two locations off the coast of Hokkaido in the Sea of Okhotsk (diamonds in Fig. 1b). One ADCP was deployed upstream of the SWC (near the Soya Strait) around the SWC axis, located ~25 km off the Hokkaido coast. This ADCP was installed with trawl-resistant bottom mount (TRBM AL-200 manufactured by Floatation Technologies) on the seafloor at a water depth of 90 m. Nearly one-year data were obtained from May 2004 to May 2005 (Fukamachi et al. 2008). The other ADCP

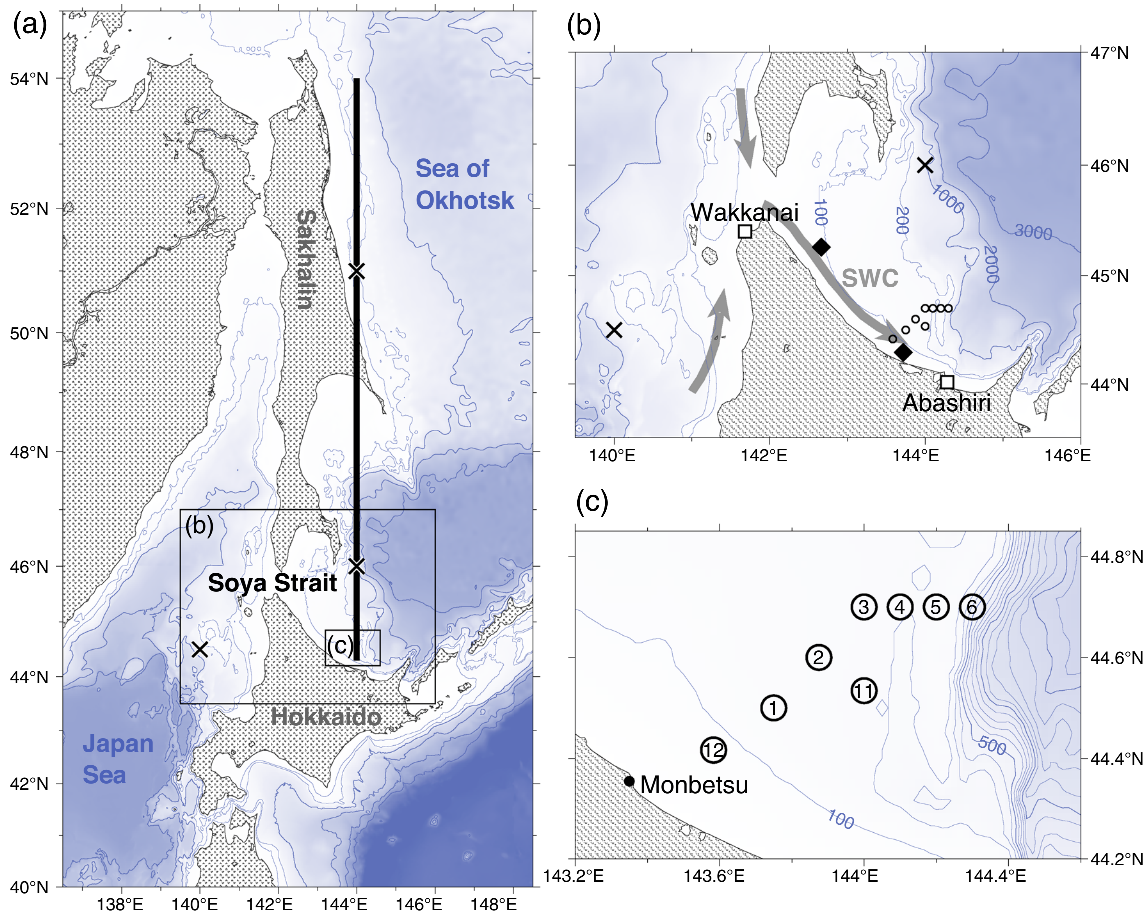

Fig. 1 (**a**) Bathymetric maps around the SWC region and its upstream area. The bathymetry data are derived from the ETOPO1. The thick solid line along the eastern Sakhalin coast indicates the integration route of the wind stress for calculation of the ATW transport. (**b**) Enlarged map of the SWC region. The solid diamonds indicate the locations of the ADCP measurements. The open squares indicate the tide-gauge stations. (**c**) Enlarged map for the vessel observation site. The open circles with a number indicate observational stations of YODA profiler. The crosses in (a) and (b) indicate the ERA5 wind and atmospheric pressure positions used in this study

was deployed downstream of the SWC, located ~ 11 km off the Hokkaido coast where the water depth is 56–59 m, and moored ~ 14 m above the ocean bottom (Fukamachi et al. 2006). The observations were conducted in four winter seasons, from November to April of 1999 to 2001. We analyzed the velocity and echo intensity data from the upstream and downstream ADCPs, mainly using the data from the first bin (the deepest bin near the seafloor) to detect the resuspension events. The center of the first bin of the upstream ADCP was positioned 7 m from the seafloor, and that of the downstream ADCP was about 20 m from the seafloor. Details of the ADCP locations and settings are summarized in Table 1.

2.2 Derivation of the ADCP backscatter strength

To detect the signal for sediment resuspension, we calculated the volume backscatter strength (SV) from the ADCP data, following Ito et al. (2017; 2020). ADCPs record reflected waves from scatters as the echo intensity, which is affected by the transmit power, the power attenuation caused by propagation losses, the characteristics of the transducer, and the properties of the receivers. By considering these factors, Deines (1999) provided the following sonar equation, which relates the backscatter strength to the echo intensity:

$$SV = C + 10\log_{10}\left(TR^2\right) - 10\log_{10}L \\ - 10\log_{10}P + 2\alpha\, R + K_c(E - E_r), \tag{1}$$

where SV (dB) is mean volume backscatter strength with reference to (4πm) $^{-1}$, C (dB) is an instrument-specific value, T (K) is the temperature of the transducer, R (m) is the range between the scatter target and the transducer, L (m) is the transmit pulse length, P (W) is the transmit power, α (dB/m) is the absorption coefficient of water, Kc (dB/count) is an echo intensity scale factor, E (counts) is the echo intensity, and Er is the reference level of E. The parameter values are from Deines (1999) : Kc=0.45 (dB/counts), C=−143.5 (dB), α=0.69 (dB/m). The value of P is derived from the voltage

Table 1 Locations and settings of the ADCPs

Location	Bottom depth (m)	Mooring period	Time interval	Bin size (m)	1st Bin from seafloor (m)	Er (counts)
Upstream[a]						
45°15.5'N 142°39.9' E	90 m	2004/05/25-2005/05/24	1 h	4	7	42
Downstream[b]						
44°19.6 0 N 143°38.8 0 E	56–59 m	1998/12/05-1999/03/27	15 min.	4	20	41
44°18.8 0 N 143°41.6 0 E	56–59 m	1999/12/12-2000/04/04	15 min.	4	20	41
44°17.6 0 N 143°43.1 0 E	56–59 m	2000/11/26-2001/03/22	15 min.	4	20	41
44°18.6 0 N 143°41.2 0 E	56–59 m	2001/11/15-2002/03/26	15 min.	4	20	42

[a]Fukamachi et al. (2008), [b]Fukamachi et al. (2006) (except for the last one)

and electric current. Ensemble values of *T*, *E*, voltage, and electric current are obtained from each ADCP observation. For *Er*, we used the value of *E* before the observation.

2.3 Vessel observation

To observe the sediment resuspension, we measured water properties including turbidity off Monbetsu in April 2022 and March 2023, using a chartered fishing boat, Seiko-maru. We used a YODA profiler (JFE Advantech) equipped with sensors measuring conductivity, temperature, pressure, chlorophyll, turbidity, and dissolved oxygen (Masunaga and Yamazaki 2014). We used turbidity, temperature, and salinity data from the downcast measurements at eight stations located between 18 and 100 km from the coast, at water depths of 80–200 m.

2.4 Meteorological and tidal data

To investigate the atmospheric conditions underlying the sediment resuspension, we used the ERA5 reanalysis dataset of 10-m wind and sea-level pressure, provided by the European Center for Medium-Range Weather Forecasts. To examine the response of the ocean to the atmospheric forcing, we used hourly sea-level data, detided by subtracting the predicted tidal oscillation at Wakkanai and Abashiri (see Fig. 1b for the locations), provided by the Japan Meteorological Agency. For these sea-level data, we removed the inverted barometric effect and applied a 48-h tide-killer filter (Hanawa and Mitsudera 1985).

3 Sediment resuspension in the upstream region of the SWC

3.1 Resuspension signals detected by ADCP data

From the ADCP backscattering measurements in the upstream region of the SWC, we could directly observe several prominent events of sediment resuspension. These events mostly occurred during September to December, as will be explained later. We show such typical cases as the time series for the vertical profiles of backscatter strength (SV) (Fig. 2a and e). On 9–10 September and 16–18 November (indicated by arrows in Fig. 2), strong SV signals intensified toward the bottom, with the signal extending close to the surface. Such patterns are typical of sediment resuspension, as demonstrated by Ito et al. (2017). We also show a time series of vertical profiles for the current speed for the same period (Fig. 2b and f). September is a month when the mean current becomes strong with a surface intensification. Diurnal tidal currents are relatively strong in the upstream region near the strait. On 9 September, when the high SV signal occurred near the bottom, the current speed was particularly enhanced by sub-inertial variations with near barotropic structure (Fig. 2c), and the current speed near the bottom exceeded 80 cm/s (Fig. 2d). November is a month when the current structure is nearly barotropic (Fig. 2f). On 16–18 November, when the high SV signal occurred near the bottom, the current was intensified with barotropic structure (Fig. 2g). Combined with the diurnal tidal currents, near-bottom currents exceeding 60 cm/s occurred during the daytime on these days. For both cases, the timing of the strong SV signal intensified toward the bottom corresponded well to that of the increased current speed.

Here we discuss the possibility of sediment dispersion from the seafloor in the bottom boundary layer, following Ito et al. (2017). We assume spherical sedimentary particles. Figure 3 shows the diagram of the suspension of sedimentary particles as functions of particle diameter and friction velocity u^*, assuming that the specific gravity of particles is 2.65 and the kinematic viscosity coefficient is 0.01 cm^2/s (the same diagram as that of Ito et al. (2017). Traction occurs when the bottom friction velocity u^* exceeds the critical friction velocities u_c^*, which can be calculated from the critical tractive force by Iwagaki (1956) (the dashed

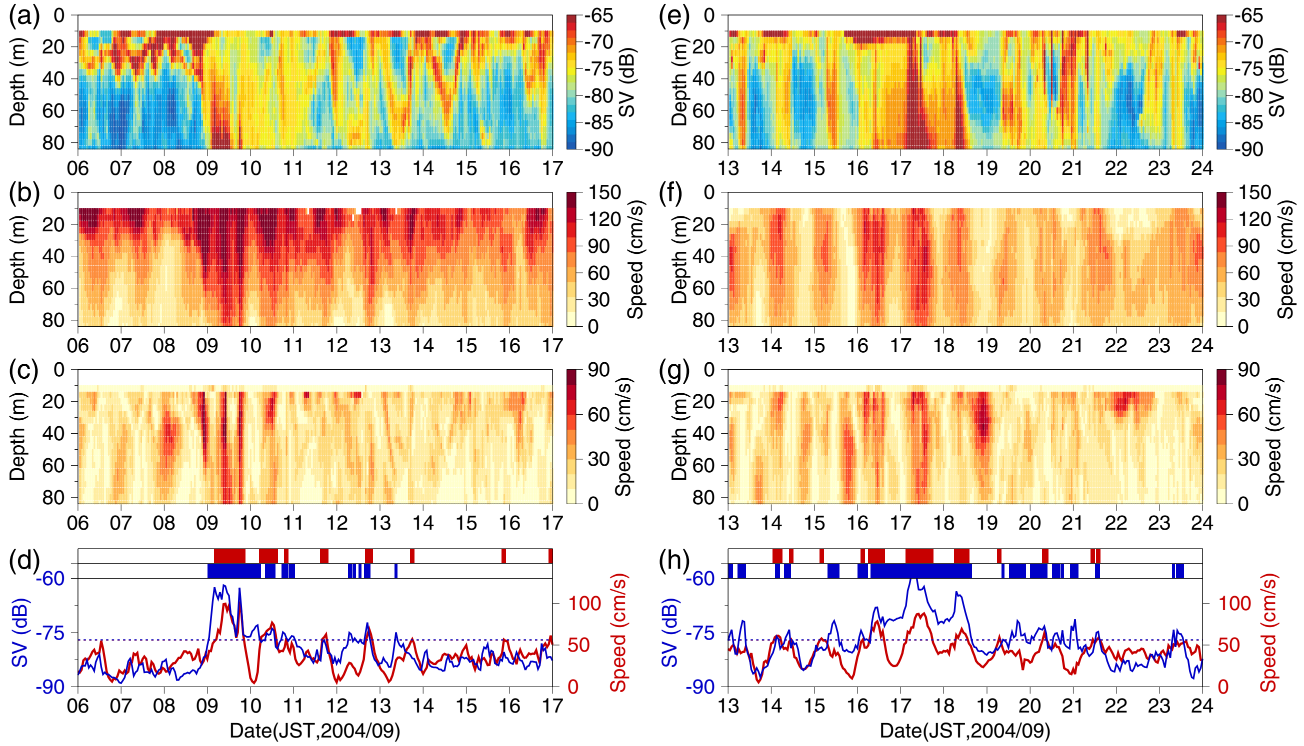

Fig. 2 Time series of typical events of sediment resuspension in the upstream region of the SWC (**a**, **b**, **c**, **d**) on 9–10 September 2004 and (**e**, **f**, **g**, **h**) on 16–18 November 2004. (a, e) The vertical profiles of the volume backscatter strength, SV. Arrows indicate the sediment resuspension timing. (b, f) The vertical profiles of the current speed. (c, g) The fluctuating component derived by subtracting the mean velocity from (b, f). (d, h) The SV and current speed from the first bin of the ADCP, with the bars in the upper panel indicating the periods when the values of SV (blue) and current speed (red) exceeded the thresholds of −80 dB and 50 cm/s, respectively

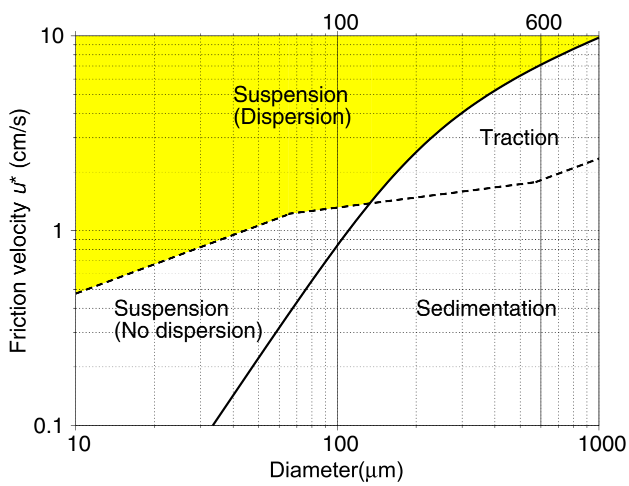

Fig. 3 Diagram of sediment suspension as a function of particle size and friction velocity u^*, following Ito et al. (2017). The dashed line represents the critical tractive force u_c^* proposed by Iwagaki (1956). The solid line represents the settling velocity w_f when the kinematic viscosity coefficient is 0.01 cm^2/s proposed by Rubey (1933). The yellow area indicates the condition under which sediment can be suspended

line in Fig. 3). Suspension keeps when the turbulent velocity exceeds the settling velocity w_f, which is provided by Rubey (1933) (the solid line in Fig. 3). Assuming that the turbulent velocity is approximated as the u^*, resuspension with vertical transport for each particle size occurs under the condition of $u^* \geq u_c^*$ and $u^* > w_f$ (the yellow area in Fig. 3). The seafloor sediment in the SWC region is mostly composed of sand particles with a grain size of 100–600 μm (Tanabe and Sakamoto 2002). For particle size of 100 μm and 600 μm, the resuspension occurs when u^* exceeds 1.3 cm/s and 7.1 cm/s, respectively, and these thresholds are converted to the velocities at the depth of the deepest ADCP bin (7 m from the seafloor) of 48 cm/s and 260 cm/s, respectively, using a law of the wall, $u(z) = \frac{u*}{\kappa} \log \frac{z}{z_0}$ with κ=0.4, z_0=3^{-6} m (the same conditions as those of Ito et al. (2017). These indicate that a part of the sediments can be suspended at the observed velocities.

For the entire period of the ADCP observation, we calculated the correlation coefficient between the current speed at the first (deepest) bin of the ADCP and SV of all bins (Fig. 4). The correlation coefficient is significantly larger closer to the seafloor. All these considered, the strong SV signals of ADCP intensified toward the bottom are due to

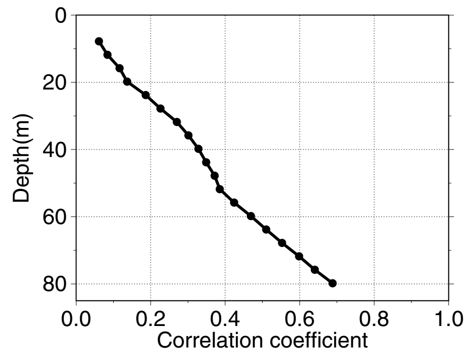

Fig. 4 The correlation coefficient between the current speed at the deepest bin of the ADCP and SV of all bins for the entire period

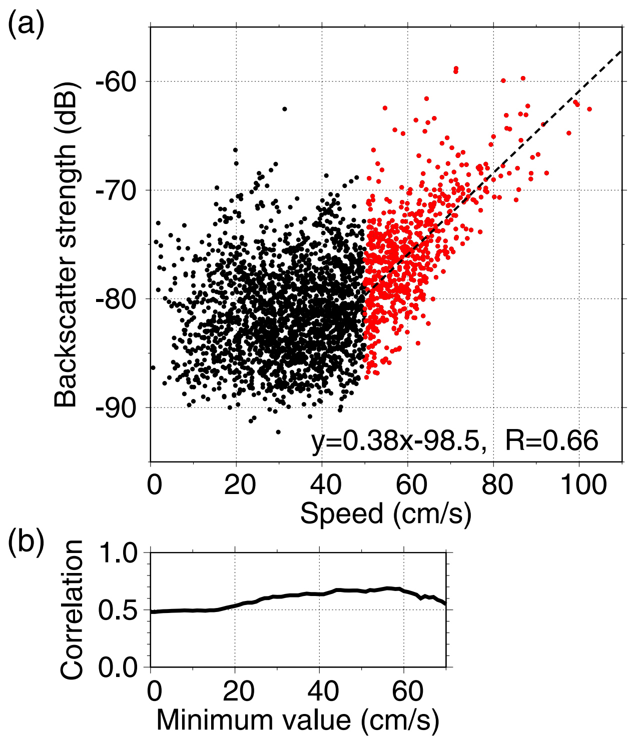

Fig. 5 (**a**) Scatter plot of the SV and current speed from the first bin of the upstream ADCP for the period from September to December 2004. Data with the current speed of exceeding 50 cm/s are shown in red. The dashed line is the regression line between the SV and current speed for all the pairs with the current speed exceeding 50 cm/s. (**b**) The correlation coefficient between the SV and current speed as a function of the setting minimum value of the current speed

the resuspension events caused by the strong current near the seafloor.

Although the resuspension in the bottom mixed layer is dynamically explained as above, the subsequent transport of sediments toward the surface should be considered separately. However, it is difficult to discuss the transport process toward the surface based solely on ADCP data from a single site, because a proper discussion requires the consideration of various factors such as the presence of upwelling (secondary circulation), stratification conditions, turbulence intensity, and the particles' specific gravity and size. Instead, to confirm the presence of resuspension near the surface, we examined the vertical velocity of suspended particles using the ADCP data, since bottom-mounted ADCPs can measure the upward and downward movement of particles with a certain degree of reliability. Enhanced vertical velocities, typically ranging from 0.5 to 3 cm/s, were detected from the bottom up to near the surface during the high backscatter strength event (not shown). This supports the occurrence that some suspended particles were transported up to near the surface, with particle size decreasing closer to the surface, as suggested in Fig. 4.

Figure 5a shows the scatter plot of the SV and current speed for the period from September to December, when resuspension events frequently occurred. According to previous ADCP observations in other regions (Ito et al. 2017, 2019), when resuspension events occur, the backscatter strength was shown to correlate with the current speed for the speed exceeding a certain value. This threshold value is regarded as the minimum value for excitation of the significant resuspension. To estimate the threshold of the current speed at which significant resuspension occurs, we calculated the correlation coefficients of the current speed with SV by setting different minimum values of the current speed for the period from September to December, when resuspension events frequently occur. Figure 5b shows the correlation coefficient as a function of the setting minimum value of the current speed. The correlation coefficient exceeds 0.6 when the minimum speed is set to 45–60 cm/s, which is consistent with the critical velocity derived from Fig. 3. From this analysis, we regard 50 cm/s as the threshold value for excitation of the resuspension. Similar threshold values for the resuspension have been reported in the east Sakhalin shelf (Ito et al. 2017) and the Chukchi coast (Ito et al. 2019). In Fig. 5a, we show the regression line between the SV and current speed for all the pairs with the current speed exceeding 50 cm/s (red plots in Fig. 5a).

Figure 2c and f show the backscatter strength and current speed from the deepest bin of the ADCP. The data demonstrate that the backscatter strength was intensified simultaneously with an increase in current speed on 9 September and on 16–18 November. The bars in the upper panel of the figures indicate the periods of large SV (blue) and large current speed (red) to visualize the correspondence between them. The threshold value of 80 dB for SV is determined by the correlation analysis with the threshold value of 50 m/s for the current speed described above (Fig. 5). This manner of visualization will be applied to the whole period later.

The seasonal variation of the mean flow observed by the ADCP is shown in Fig. 6, in which velocities were averaged over 30 days. The surface velocity has a large seasonal variation, with the maximum velocity reaching more than 110 cm/s in September and the minimum velocity being approximately 30 cm/s in February. In contrast, the near-bottom velocity shows much less seasonal variation, with a near-constant velocity of 40–50 cm/s from June to November and a minimum of approximately 30 cm/s in January and February.

Figure 7 shows the whole time series of the SV and current speed from the deepest bin of the ADCP, with values larger than the thresholds indicated by the bars in the same manner as in Fig. 2d. Each row of Fig. 7 corresponds to a 1-month time series. During the period from September to December, strong current events lasting a few days at a time (synoptic scale) occurred two or three times per month; specifically, on September 1–2, 9–10, 20–22, October 2–3, 23–26, November 7–10, 16–18, 25–29, and December 8–13, 2004. Correspondingly, the backscatter strength simultaneously increased near the bottom.

On the other hand, because of the strong diurnal tidal currents near the Soya Strait (Ebuchi et al. 2006), the current speed sometimes exceeded the threshold value when the southeast phase (downstream direction) of the tidal currents add to the strong mean flow, as often shown from June to August. Even for such cases, however, the increase in backscatter strength is limited to some extent and less prominent than in the cases of synoptic strong current events. This is because the large velocity increase by the tidal current continues for only several hours at most, and the relatively short duration of the intensification is not enough to induce a prominent sediment resuspension.

In addition to the sediment resuspension signal, the ADCP backscatter strength can also detect the zooplankton and frazil ice (Ito et al. 2017). In Fig. 7, high SV events that do not correspond to the current fluctuations sometimes occurred mainly from March to May. These events are likely caused by the zooplankton activities, since this period is the spring bloom season. In Fig. 2a, the SV exhibits a V-shaped variation with a diurnal cycle characterized

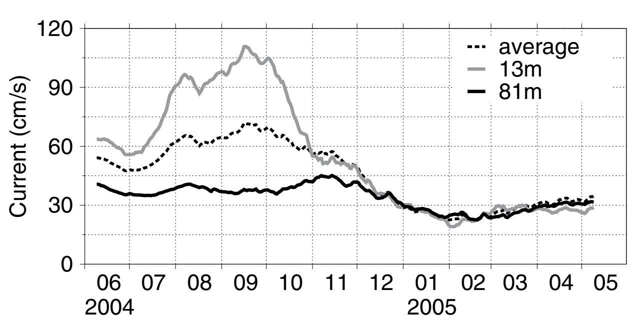

Fig. 6 Seasonal variation in the current speed observed by the upstream ADCP with a running 30-day mean. Near-surface velocity at the depth of 13 m (gray solid line), near-bottom velocity at the depth of 7 m from the bottom (black solid line), and vertically averaged velocity (black dotted line) are shown

by a strong signal in the surface layer during the nighttime and a strong signal near the bottom during the daytime. The timings of the upward and downward shifts of high SV correspond to sunset and sunrise, respectively. This variation is considered as the diurnal vertical migration (DVM) of zooplankton. Such DVM signals from the ADCP backscatter strength have been reported in many studies (e.g. Cisewski et al. 2010; Inoue et al. 2016; Liu et al. 2022). The ADCP backscatter strength would become strong in the lower layer with the downward migration of zooplankton during the daytime. If the peak of the diurnal tidal current coincides with the daytime when the zooplankton stays near the seafloor, the current speed and SV near the bottom would show some correlation. To investigate the effect caused by zooplankton on SV, we removed the SV component with a 24-hour periodicity related to the behavior of zooplankton: high SV near the bottom during the daytime and high SV near the surface during the night time (see the Appendix for the details of the processing). The correlation coefficient between the SV without the 24-hour periodic component and the current speed has values comparable to those for the raw SV case (Fig. 15 in the Appendix). This result further supports that the strong backscattering signals are due to the sediment resuspension caused by the strong current events.

3.2 The conditions of sediment resuspension

According to our analysis, resuspension occurs when the strong currents event lasts a few days (Fig. 7). In this subsection, we examine the atmospheric conditions that enhanced the bottom current and thus induced the sediment resuspension. We also explore how the bottom current is intensified.

Figure 8 shows the time series of key quantities for the strong current and high SV events, around 9–10 September and 16–18 November 2004. The wind and the atmospheric pressure at the shelf edge in the Japan Sea (Fig. 8a and f) and Okhotsk Sea (Fig. 8b and g) across the Soya Strait indicate that a cyclone passed through the area around the Soya Strait 1 or 2 days before the resuspension event, bringing strong southerly winds exceeding 10 m/s in both cases.

The SWC is primarily driven by the sea-level difference between the Japan Sea and Okhotsk Sea (Ohshima 1994). When the sea-level difference occurs across the Soya Strait, a mass flux into the Okhotsk Sea is induced in the strait. This mass flux excites the coastal trapped wave (CTW), which propagates along the Hokkaido coast, thereby the coastal trapped flow, the SWC, is established (Ohshima 1994). Similarly, a mechanism of synoptic wind-induced variation of the SWC has been proposed by Ebuchi et al. (2009). When the southerly winds blow in both oceans centering around the strait, the sea level rises along the coast of Hokkaido on the Japan Sea side by the onshore-ward

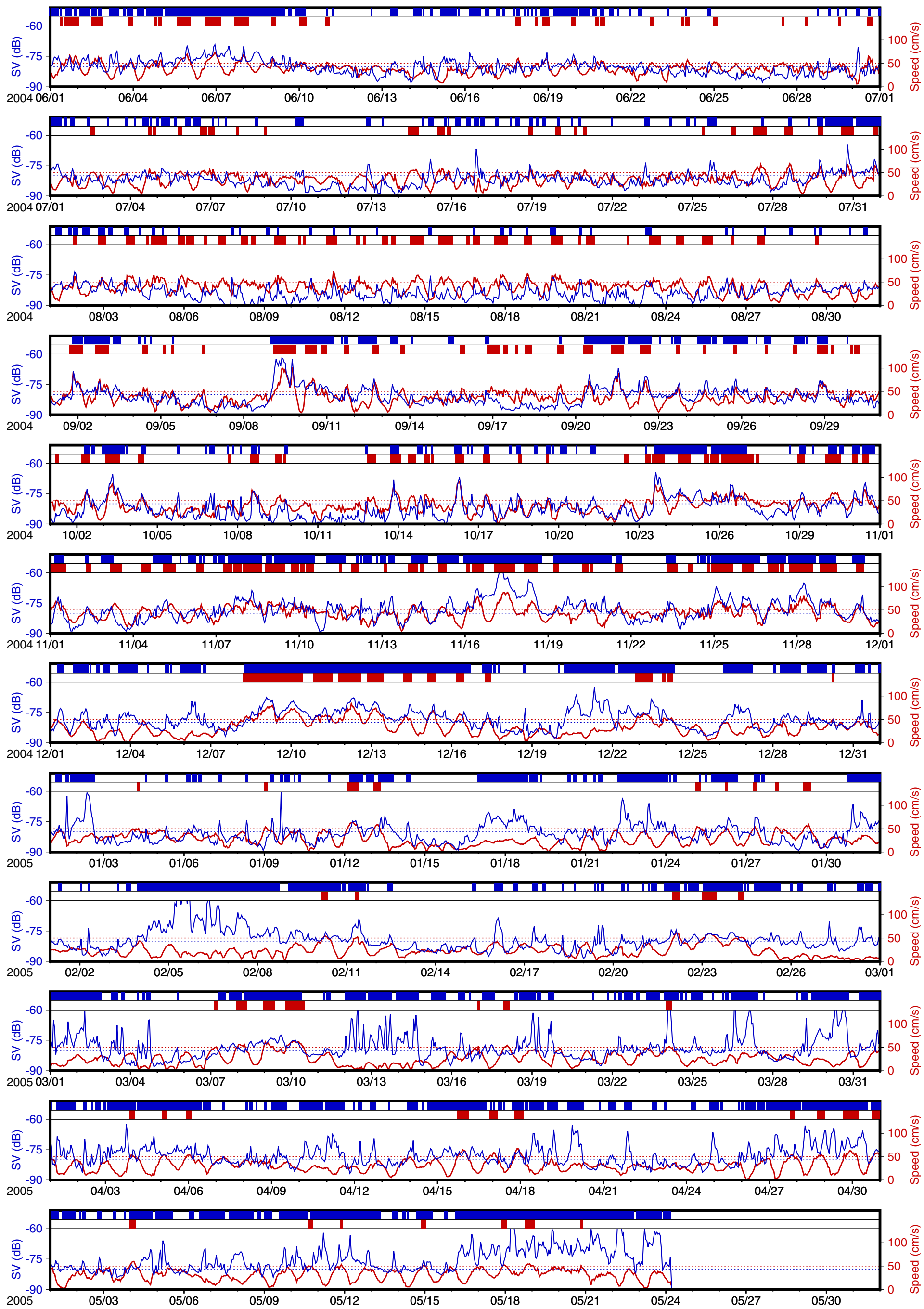

Fig. 7 Whole time series of the SV (blue line) and current speed (red line) from the first bin of the upstream ADCP. The bars in the upper panel indicate the periods of values exceeding thresholds in the same manner as Fig. 2d. Each row corresponds to 1-month time series

Ekman transport, while it drops on the Okhotsk Sea side by the offshore-ward Ekman transport. As a result, the sea-level difference between the strait increases, inducing the enhanced flux from the Japan Sea to the Okhotsk Sea, thereby strengthening the SWC. The northerly winds opposingly reduce the SWC. Since the sea level rise or drop by the Ekmann transport is associated with the CTW and the variation propagates with the coast to the right (from the south in the Japan Sea and from the north in the Okhotsk Sea), the variation of the SWC occurs with a lag of one or two days against the wind variation, as shown by observational data in Ebuchi et al. (2009).

Referring to these previous investigations, we examine an ocean response to the wind forcing during the strong currents and high SV events. Figure 8c and h show the sea-level anomalies at Wakkanai (Japan Sea side) and Abashiri (Okhotsk Sea side) and their difference, and Fig. 8d and i show the barotropic component of the current, calculated as the vertical average of alongshore current component with tidal components removed by 25-hour running mean.

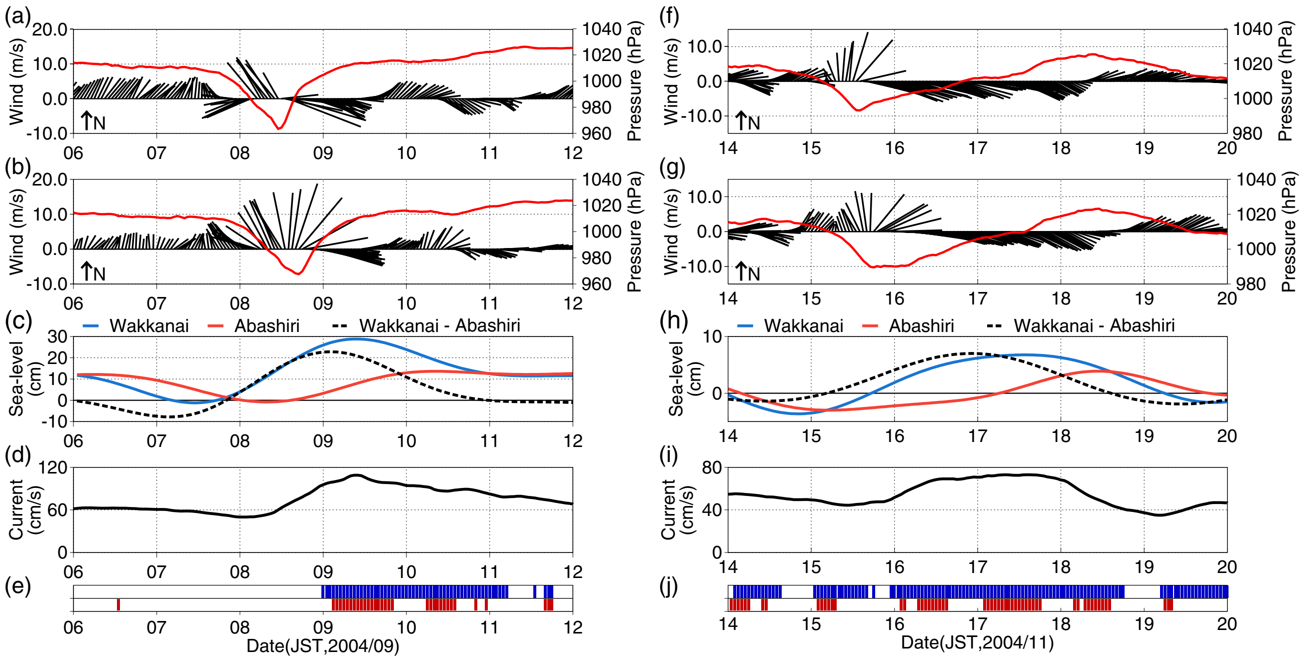

Fig. 8 Time series of quantities related to the wind-induced current variation in the upstream region of the SWC for strong current events (**a**–**e**) on 9–10 September 2004 and (**f**–**j**) on 16–18 November 2004; the wind (black vector) and atmospheric pressure (red line) at the shelf edge (**a** and **f**) in the Japan Sea and (**b** and **g**) in the Okhotsk Sea across the Soya Strait, (c and h) sea-level anomaly at Wakkanai (Japan Sea side; blue line) and Abashiri (Okhotsk Sea side; red line) and their difference (dashed line), (**d** and **i**) the vertical average of the alongshore current component (74°counterclockwise from east) with the tidal components removed by 25-hour running mean, and (**e** and **j**) the periods when the SV (blue bar) and the current speed (red bar) values exceeded the thresholds in the same manner as Fig. 2d

Simultaneously with the increase in wind speed, the sea level at Wakkanai increased, and that at Abashiri decreased, resulting in an increase in the sea-level difference and an enhancement of the barotropic current.

These variations indicate that the current variations in the SWC region occur by the mechanism described by Ebuchi et al. (2009) and Ohshima (1994). Specifically, a continuous northward blowing wind induces a sea-level difference across the strait, resulting in an increased volume flux from the Japan Sea to the Okhotsk Sea. This flux is trapped by the Hokkaido coast and propagates downstream as CTWs, leading to an intensification of the current. Since the width of the continental shelf along the Hokkaido coast (50–100 km) is sufficiently wider than the internal radius of deformation, the structure of the CTWs near the Hokkaido coast is considered to be barotropic (Huthnance 1978). A rough estimate of the internal radius for strong stratification season in this region is 5–6 km, assuming a two-layer structure with an upper layer 20 m thick (σ_θ=25.0) and a lower layer extending to a depth of 150 m (σ_θ=26.5). Therefore, southerly wind events are expected to induce an almost vertically uniform increase in velocity (Fig. 2b and f). This series of events finally leads to an intensification of the backscatter strength around the peak of the barotropic current (Fig. 8e and j).

3.3 Seasonal variation of the resuspension event

Next, we investigated the seasonal variation of resuspension events caused by strong southerly winds in the upstream region of the SWC. Figure 9a shows the monthly frequency of resuspension events that occurred from Jun 2004 to May 2005, defined as accumulated hours when the hourly ADCP data show that the current speed of ≥60 cm/s and SV of ≥−75 dB (black bar) and the current speed of ≥50 cm/s and SV of ≥−80 dB (gray bar). Figure 9b shows the monthly frequency of the strong southerly wind event in the same period. A strong wind event is defined as an event when the southerly wind component exceeds 10 m/s (black) and 9 m/s (gray) both in the Japan Sea and Okhotsk Sea sites based on the ERA hourly wind data, with the Okhotsk Sea wind following the Japan Sea wind within 2 h. If multiple events occur within 2 days, these events were counted as one event. These definitions are based on our analysis in the previous section (Sect. 3.2). Figure 9a demonstrates that resuspension events actively occurred from September to December. Figure 9b shows that the southerly wind event exhibits similar seasonal variation. These data suggest that a high activity of atmospheric disturbance with strong southerly winds from September to December causes frequent occurrence of the resuspension event during that period in the upstream region of the SWC. We then examined whether

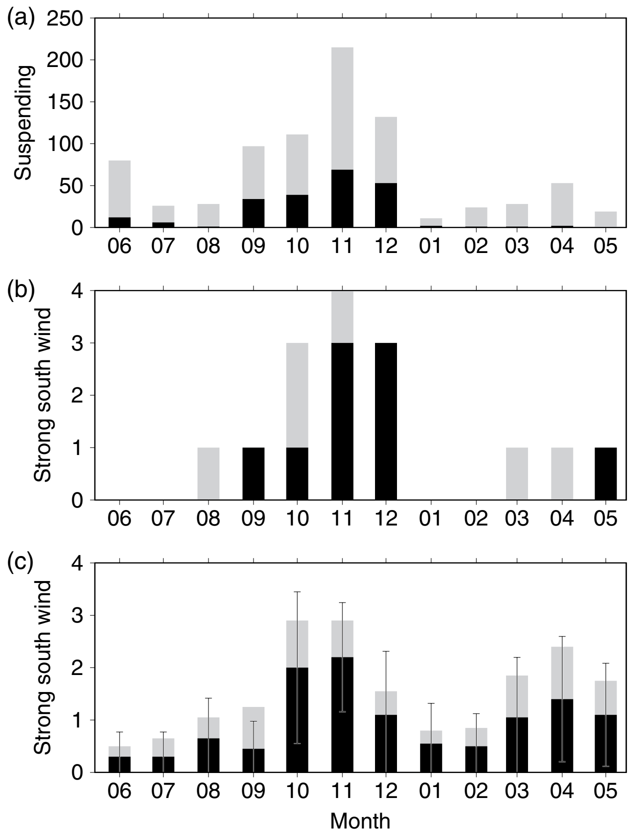

Fig. 9 (**a**) Monthly frequency of the sediment resuspension event in the upstream region of the SWC, detected by the ADCP observed from June 2004 to May 2005. (**b**) Monthly frequency of the southerly wind event in the area across the Soya Strait, derived from the ERA5 wind data in the same period of (**a**). (**c**) Climatology for the monthly frequency of the southerly wind event from 2000 to 2022, derived from the ERA5 wind data. See the text for the detailed definition of the monthly frequency of the sediment resuspension and southerly wind events

such seasonal variation was specific to our observation period (2004–2005) or commonly occurred in other years. Figure 9c shows the climatology for the monthly frequency of southerly wind events derived from the ERA wind data from 2000 to 2022 in the same manner as in Fig. 9b. The climatology exhibits seasonal variation similar to that in 2004–2005. We thus infer that resuspension events occur frequently during the period from September to December every year in the upstream region of the SWC.

The wind climatology (Fig. 9c) suggests a relatively high occurrence of resuspension events during the period from March to May as well. In fact, on 7–9 March 2005, an increase in backscatter strength (Fig. 7), considered to be a resuspension event, was induced by a strong southerly wind event. With the exception of that event, the maximum velocity remained relatively low, 60 cm/s at most, and prominent high backscatter events did not occur during the period from March to May, despite the temporary occurrence of southerly wind events. This lack of a prominent backscatter event is likely due to the smaller mean flow of the SWC in this season, which is in contrast to the relatively strong mean flow in autumn, as shown in Fig. 6. In this season, the current speed is unlikely to reach a velocity that is high enough to cause a clear sediment resuspension, even if the wind-forced current is added to the mean flow. The volume transport and velocity of the SWC reach a maximum in August (Ohshima et al. 2017). However, the absence of strong southerly wind events makes August less occurrence month of sediment resuspension events.

4 Sediment resuspension in the downstream region of the SWC

4.1 Resuspension event detected by ADCP data

The ADCP observations were also conducted in the downstream region of the SWC to obtain information on sea ice thickness and drift during sea ice season (Fukamachi et al. 2003, 2006). Although the data acquisition was limited to the period from December to March, data were obtained for four winter seasons from 1998 to 2002. We calculated the backscatter strength using the same method as described in Sect. 2.2. The upward-looking ADCPs were installed at about 20 m above the seafloor at each mooring. The concentration of particles with large specific gravity decreases with distance from the bottom within the bottom mixed layer (Furuichi et al. 2019). Hence, the detection capability was reduced and only prominent resuspension events could be extracted.

From the analysis of the ADCP data for the four winter seasons, four distinct events were identified in which the backscatter strength increased synchronously with the increase in current speed. These events were regarded as sediment resuspension events (see Online Resource 1). Figure 10 shows the time series of key quantities for two events as examples. The key quantities are wind and atmospheric pressure in the Okhotsk Sea at (a and g) central Sakhalin coast (upstream of the ESC) and (b and h) the southern tip of Sakhalin, (c and i) Ekman transport integrated along the east coast of Sakhalin (the details will be explained later), (d and j) sea-level anomalies at Wakkanai (the Japan Sea side) and Abashiri (the Okhotsk Sea side) and their difference, (e and k) the vertical average of the alongshore velocity with the tidal components removed by 25-hour running mean, and (f and l) the current speed (cm/s) and backscatter strength (dB) at the first bin of the ADCPs.

In the upstream region of the SWC, the strong southerly winds enhance the sea-level difference and the current speed of the SWC, causing the intensification of the backscatter strength (sediment resuspension). By contrast, in the downstream region of the SWC, the strong northerly winds are

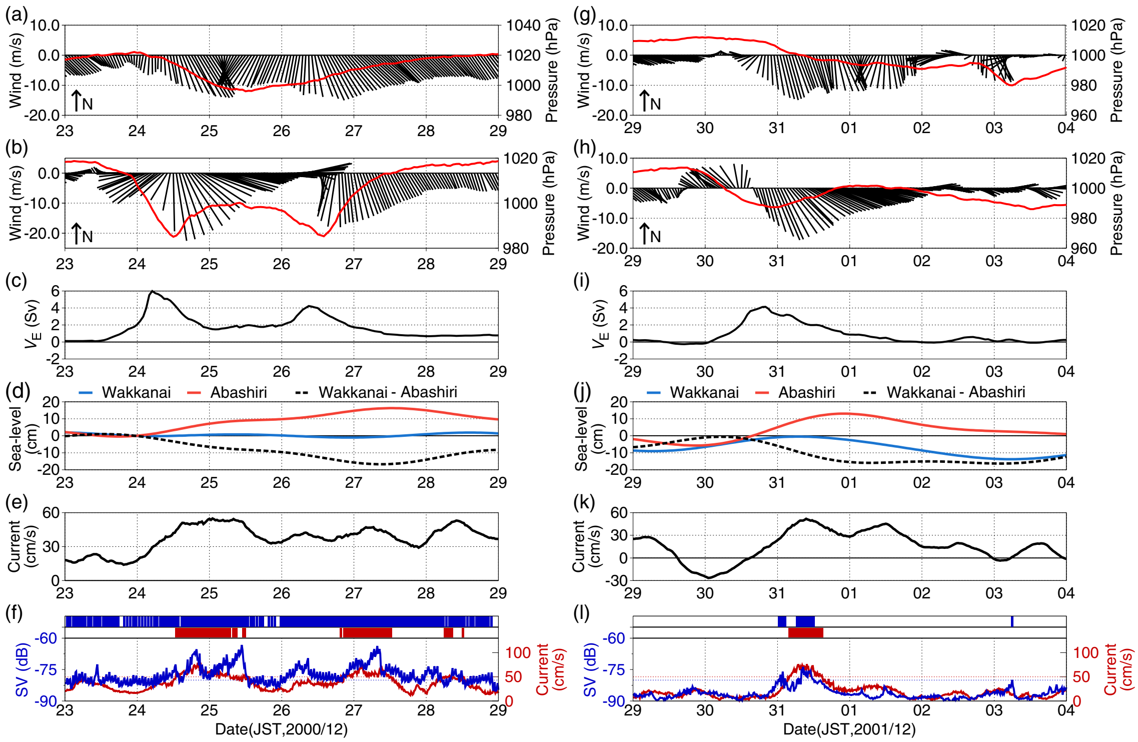

Fig. 10 Time series of quantities related to the wind-induced current variation in the downstream region of the SWC for strong current events (**a**–**f**) on 24–27 December 2000 and (**g**–**i**) on 31 December 2001); the wind (black vector) and atmospheric pressure (red line) (**a** and **g**) at central Sakhalin coast (the ESC region) and (**b** and **h**) at the southern tip of Sakhalin, (**c** and **i**) Ekman transport integrated along the east coast of Sakhalin to Hokkaido coast, (**d** and **j**) sea-level anomaly at Wakkanai (Japan Sea side, blue line) and Abashiri (Okhotsk Sea side, red line) and their difference (dashed line), (**e** and **k**) the vertical average of the alongshore current component (38° counterclockwise from east) with the 25-hour running mean, and (f and l) the current speed (cm/s) and backscatter strength (dB) at the first bin of ADCP with the SV (blue bar) and current speed (red bar) values exceeding the thresholds, in the same manner as Fig. 2d

likely responsible for the intensification of the current speed and backscatter strength, and the sea-level difference does not increase during the events.

4.2 Possible mechanism of strong current events

One of the mechanisms by which the northerly wind strengthens the current along the northeastern coast of Hokkaido is the CTWs trapped over the continental shelves off the east coast of Sakhalin and Hokkaido induced by the alongshore wind stress. If this is the case, the current and sea level would be enhanced off Hokkaido coast with a lag from the wind. In fact, the sea level at Abashiri rose with a delay of approximately 1 day following the strong northerly winds. To examine the excitation of CTWs, we calculated the sum of Ekman transport by the alongshore wind stress τ in the upstream region, defined as

$$V_{\mathrm{E}} = \int \frac{\tau}{\rho} \mathrm{d}x \tag{1}$$

with the integration route from the east Sakhalin coast to the Hokkaido coast (indicated by a thick solid line in Fig. 1a), where ρ is the density of sea water. V_{E} can be a good index for forcing of CTWs in the ESC region (Ohshima and Simizu 2008). The peak of the current velocity in the downstream region of the SWC (Fig. 10e and k) followed the peak of V_{E} with a lag of about a half day (Fig. 10c and i).

According to Mizuta et al. (2005), the phase speed of the first mode CTW on the east coast of Sakhalin ranges from 5.4 to 8.5 m/s (290–740 km/day). The distance from central Sakhalin to the downstream region of the SWC is approximately 600 km. Assuming the phase speed of 5.4–8.5 m/s, it would take roughly 1 day for the CTW to reach the coast of the downstream region. Considering that the delay of the velocity peak from the V_{E} peak is shorter than a day, a strong current causing a resuspension event in the downstream region is likely caused more by the forced CTW, excited by local northerly winds around the ADCP station. The sea level at Abashiri gradually increased even after the peak of the current velocity. We attributed this increase to the continuous propagation of the first mode CTW from upstream off the east coast of Sakhalin, since the contribution of the first mode CTW to the sea-level variation is much larger than those of the lower modes. In response to this gradual sea-level rise, however, the current was not intensified and thus the resuspension is unlikely to have occurred, because the first mode CTW does not have a large amplitude of velocity near the coast.

There were two cases of high SV events (Fig. 11e and j) in the downstream region in response to a strong southerly wind (Fig. 11a, b and f, and 11g) that could excite the resuspension in the upstream region, on 7 January 2000 and 22 January 2002. However, no increase in current speed was observed for either case (Fig. 11d and i), suggesting that local resuspension did not occur and that high turbidity water generated by the resuspension in the upstream region had been advected. In the downstream region of the SWC, both the mean and sub-inertial currents, originating from the strait, are considered to be weakened (Karaki et al. 2018). Therefore, local resuspension events by the southerly winds are unlikely to occur.

4.3 High turbidity water detected by Yoda profiler in the downstream region of the SWC

Cross-section observations of turbidity were conducted by a fishing vessel to assess sediment resuspension directly in the area near the downstream ADCP station (Fig. 1c circle). The observations were carried out in early spring of 2022 and 2023 after sea ice had melted. High turbidity water could be detected just above the seafloor at depths of 100 to 200 m in both years (Fig. 12a and c). The vertical sections of temperature, salinity, and density (Fig. 12b and d) show that the SWC water with high temperature, salinity, and density underlay the winter water formed in sea-ice season with temperatures below 0 °C. The distribution of high turbidity water observed just above the seafloor appears to correspond to that of the SWC water with a potential density of greater than 27.0σ_θ. In the SWC region, water with a potential density greater than 26.8σ_θ, which can be a component of OSIW, is present from March to July (Watanabe and Wakatsuchi 1998; Ohshima et al. 2017). Therefore, high turbidity water in the SWC region could be supplied to OSIW during that period.

To investigate whether the bottom high turbidity water was generated by local resuspension, we analyzed the occurrence of strong wind events and sea-level fluctuation (Fig. 13). No significant peak in sea-level difference between Wakkanai and Abashiri was observed in either case. This result suggests that the enhancement of the SWC by an increase in the sea-level difference, as observed in the upstream region, did not occur. With regard to the wind variations, in the case of 2023, a continuous strong northerly wind of ~10 m/s was blowing for 2 days before the observation (Fig. 13e and f), as also represented by a large increase in the V_E (Fig. 13g). Subsequently, the sea level at Abashiri increased 1 day before the observation, suggesting an intensification of the current velocity by the same mechanism as described in the previous section (Sect. 4.2). In the case of 2022, a weaker northerly wind blew 2–3 days before the observation and a weak southerly wind blew just before the observation (Fig. 13a and b). The local resuspension was likely much weaker than in the case of 2023, which is consistent with weaker signals of high turbidity water (Fig. 12a). These results suggest that the local resuspension

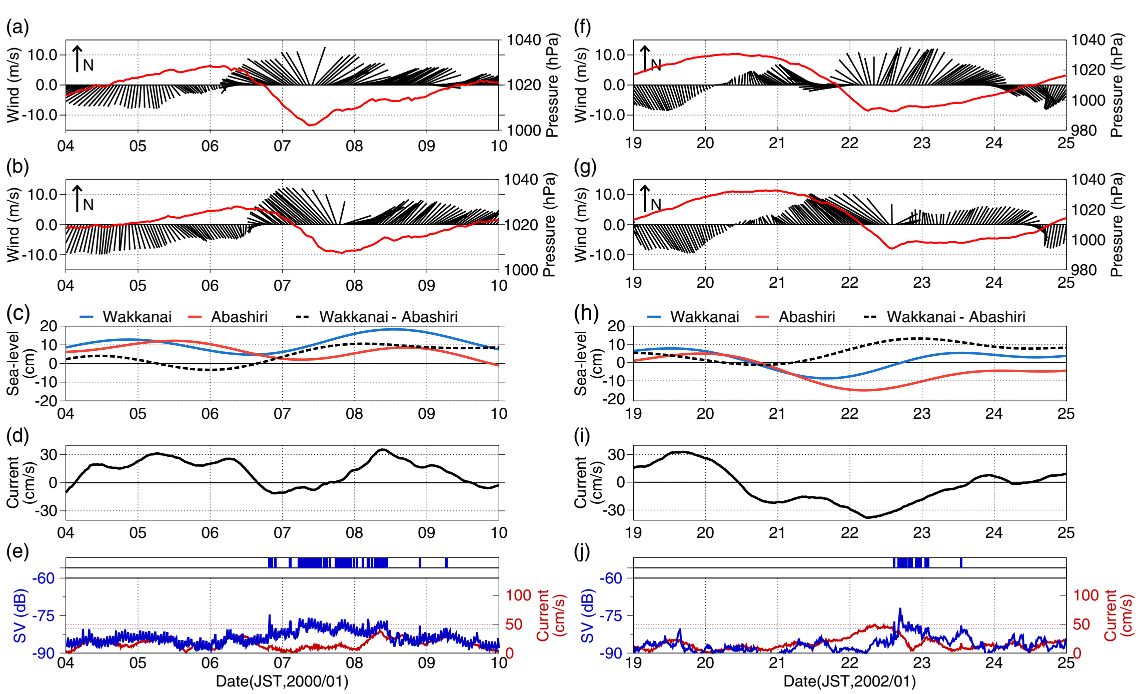

Fig. 11 Same as Fig. 8 but for the cases of strong southerly wind events with strong backscattering occurring in the downstream region, (**a**–**e**) on 7 January 2000 and (**f**–**j**) on 22 January 2002. The alongshore components (**d** and **i**) are in the same direction as those in Fig. 10 (**e** and **k**)

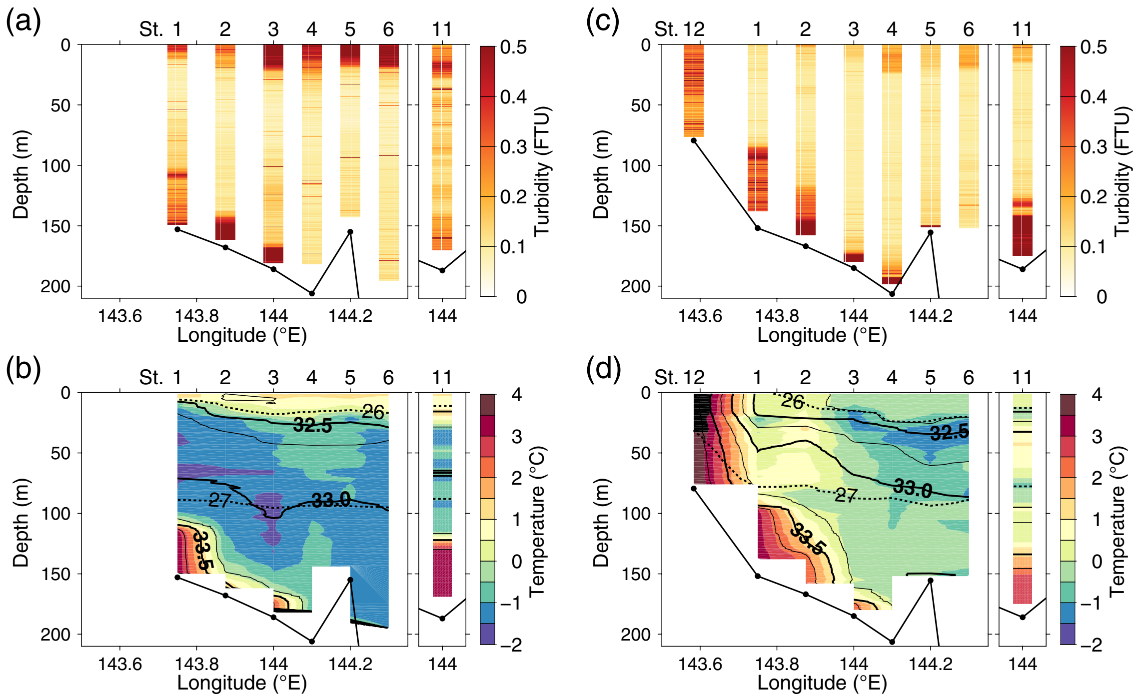

Fig. 12 Vertical sections of (**a** and **c**) turbidity, and (**b** and **d**) temperature (color), salinity (solid contours), and density (dashed contours) measured off Monbetsu (**a** and **b**) on 16 April 2022 and (**c** and **d**) on 26 March 2023. The observational stations are indicated in Fig. 1c

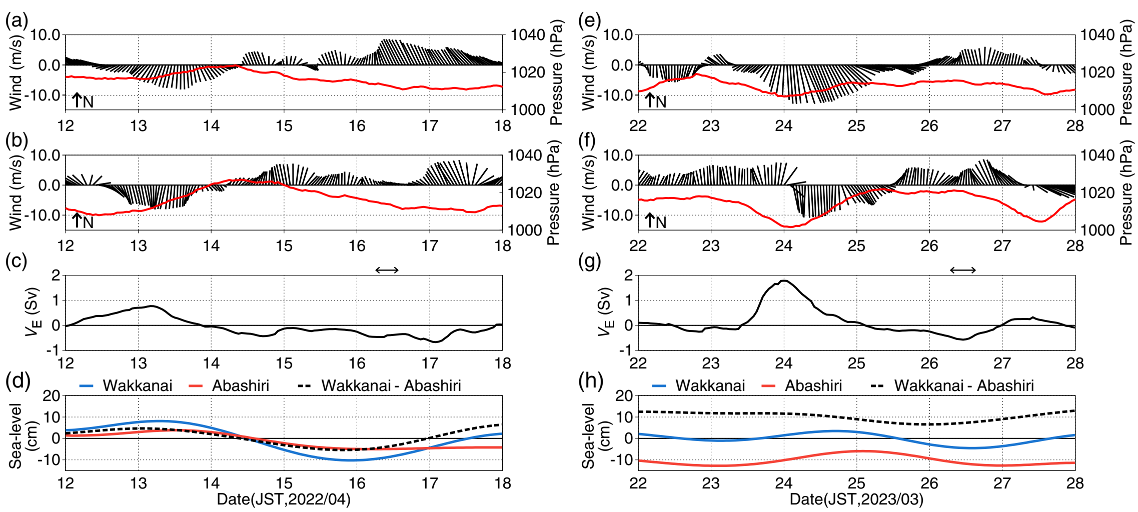

Fig. 13 Time series of quantities related to the wind-induced current variation for the cases of the vessel observations off Monbetsu on (**a**–**d**) 16 April 2022, and (**e**–**h**) 26 March 2023 represented in the same manner as Fig. 10 (a–d). Arrows indicate the vessel observation timing

associated with strong northerly winds generates the bottom high turbidity water.

5 Summary and discussion

In this study, we investigate the occurrence of sediment resuspension and its seasonal variations, based on the information of ADCP backscatter strength and turbidity measurement. We found that the backscatter strength could detect clear signals of the resuspension (large SV profile intensified toward the seafloor) in the upstream and downstream regions when the current speed exceeds ~ 0.5 m/s (Fig. 2a and e). The results suggest that the SWC region can also be a key region for the origin of micro-nutrients such as iron via the sediment resuspension in the Sea of Okhotsk.

In the upstream region of the SWC, resuspension events frequently occur from September to December, because the bottom current is intensified by a superposition of the seasonal strong mean current and strong current events by frequent synoptic atmospheric disturbances. The strengthening of the SWC occurs under the condition of strong southerly winds exceeding ~ 10 m/s on both sides of the strait. Ekman transport induced by the southerly winds raises the sea level on the Japan Sea side and decreases the sea level on the Okhotsk Sea side, resulting in an increase in the sea-level difference between the two oceans and consequent enhancement of the mass flux from the strait (Ebuchi et al. 2009). Once the sediment resuspension occurs near the bottom, upward movements of sediment might be enhanced by the Ekman convergence of the bottom boundary layer associated with the SWC (Ohshima 1986; Ishizu et al. 2006).

The climatology of the frequency of such strong southerly wind events suggests that the high frequency of the resuspension in September to December commonly occurs every year. A resuspension can occur in other seasons whenever the current speed is intensified by such strong wind events. From June to August, in spite of the strong seasonal mean current, the resuspension occurs less frequently because there are fewer atmospheric disturbances with strong southerly winds. From January to May, the resuspension is also not frequent because of weaker seasonal mean current.

In the downstream region, sediment resuspension events are mainly induced by the CTWs excited by northerly winds over the continental shelf, and not by the intensification of the SWC, which is in contrast with the case of the upstream region. The direct shipboard turbidity observations in the downstream region detected strong turbidity signals just above the seafloor, further supporting the occurrence of sediment resuspension. It is noted that the mechanism of the strong current occurrence differs between the upstream and downstream regions, while the sediment resuspension could occur in both regions.

Based on direct turbidity observations and the comparison between the resuspension signal of ADCP data and monthly climatology of the potential density (Ohshima et al. 2017), the density of high turbidity water generated by the sediment resuspension would have a range about 26.4–27.2σ_θ. The SWC water with a potential density of greater than 26.8σ_θ has been proposed to contribute to the formation of the OSIW (Watanabe and Wakatsuchi 1998; Itoh et al. 2003). However, as pointed out by Mensah et al. (2024), dense SWC may contribute more to the water around the Kuril Straits and coastal Oyashio water, because it is trapped over the continental shelf. The high iron concentration in the coastal Oyashio water (Nishioka et al. 2011, 2014, 2021) possibly originates from the SWC water.

Resuspension events still occur during the sea ice season from January to March. Therefore, if the transport of sedimentary particles to near the surface, as suggested in Fig. 2a and e, occurs during the sea ice season, iron-containing sediments are possibly incorporated into sea ice at the time of resuspension events. This incorporation from the SWC water might contribute partly to the high iron concentration in sea ice in the southern part of the Okhotsk Sea observed by Kanna et al. (2014).

To identify the substances in water with high turbidity and/or high backscatter strength, direct water sampling and analysis, as done by Imai et al. (2024), are indispensable. Such observation combined with the simultaneous acoustic (such as ADCP) backscattering observation will be required in the future.

Appendix: separation of the diurnal vertical migration (DVM) signal of zooplankton from backscatter strength

Precisely separating the signal of sediment resuspension and that of zooplankton from the ADCP backscatter strength data is impossible. However, we are able to extract and remove the DVM component, which shows the precise 24-hour cycle characterized by a strong signal in the bottom layer during the daytime and a strong signal in the surface layer during the night time. The analysis period was set to September-October 2004, when there were frequent resuspension events and the DVM pattern is similar over the period (Fig. 14a). The DVM pattern was extracted by mode expansion of the 18 vertical layers×24-hour data as one spatial vector in the complex empirical orthogonal function (CEOF) analysis.

Based on the results of the analysis, the component that represents the DVM variation was obtained as the CEOF first mode with a 41% contribution (Fig. 14d). Then, to provide the time series of SV that suppresses the effect of the DVM to some extent (Fig. 14c), the time series of the first mode CEOF (Fig. 14b) was subtracted from the original time series of backscatter strength (Fig. 14a). Assuming that the zooplankton contribution was thus removed by this subtraction to some extent, we re-examined the relationship between the current speed and backscatter strength in the bottom layer and new plots are shown in Fig. 15. For all the pairs with a current speed exceeding 56 cm/s, the correlation obtained is similar to that of the original data.

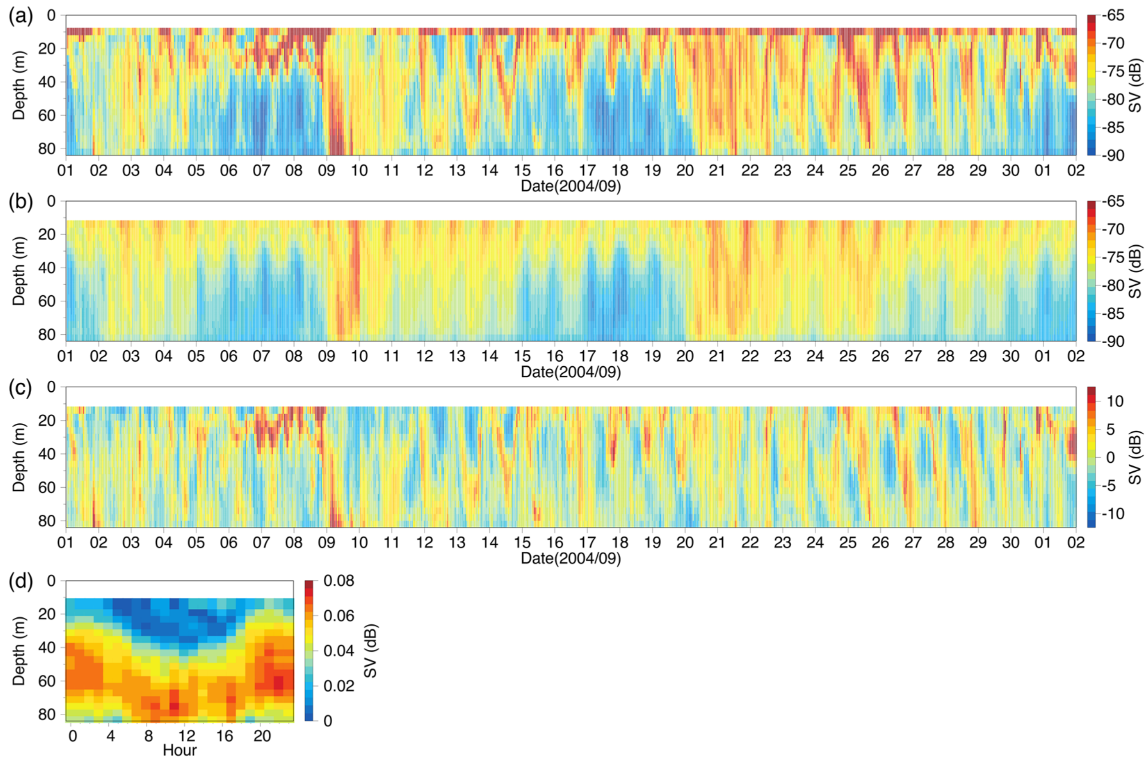

Fig. 14 (**a**) Time series of the vertical profiles of backscatter strength SV of the upstream ADCP during the period from September to October 2004. (**b**) The reconstructed time series of the first mode CEOF. (**c**) The time series of the SV that suppresses the effect of DVM, where the original SV (Fig. 14a) is subtracted by the first mode CEOF (Fig. 14b). (**d**) The structure of the first mode CEOF

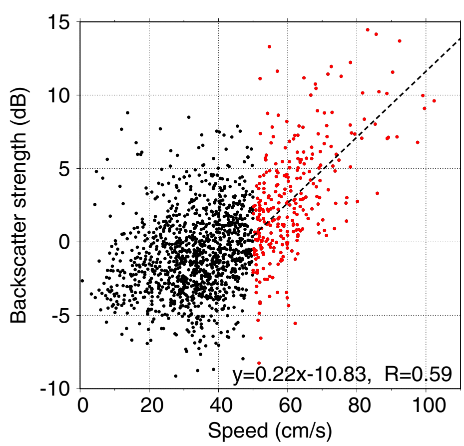

Fig. 15 The scatter plot of the SV with the first mode CEOF subtracted (Fig. 14c) and the current speed from the first bin of the upstream ADCP for the period from September to October 2004. Data with the current speed exceeding 50 cm/s are shown in red. The dashed line is the regression line between the SV (Fig. 14c) and the current speed for all the pairs with the current speed exceeding 50 cm/s

Supplementary Information The online version contains supplementary material available at https://doi.org/10.1007/s10872-025-00780-w.

Acknowledgements We are deeply indebted to the captain of F/V Seiko-maru, Masashi Matsui, for the shipboard observations and to Seiji Katakura (Monbetsu city) and Shizuaki Takeda (Monbetsu Fishery Cooperative) for their logistic support. We also thank Vigan Mensah and Mariko Honda for their help in the shipboard observations. This work was supported by Grants-in-Aids for Scientific Research (24K17121, 20K20933, 20H05707). The figures were produced with the Generic Mapping Tools (GMT) and gnuplot.

Declarations

The authors have no conflict of interest.

References

Cisewski B, Strass VH, Rhein M, Krägefsky S (2010) Seasonal variation of diel vertical migration of zooplankton from ADCP backscatter time series data in the Lazarev Sea, Antarctica. Deep-Sea Res I 57:78–94. https://doi.org/10.1016/j.dsr.2009.10.005

Deines KL (1999) Backscatter Estimation Using Broadband Acoustic Doppler Current Profilers. Proceedings of the IEEE 6 Working Conference on Current Measurements:249–253

Ebuchi N, Fukamachi Y, Ohshima KI, Shirasawa K, Ishikawa M, Takatsuka T, Daibo T, Wakatsuchi M (2006) Observation of the Soya warm current using HF ocean radar. J Oceanogr 62:47–61. https://doi.org/10.1007/s10872-006-0031-0

Ebuchi N, Fukamachi Y, Ohshima KI, Wakatsuchi M (2009) Subinertial and seasonal variations in the Soya warm current revealed by HF ocean radars, coastal tide gauges, and bottom-mounted ADCP. J Oceanogr 65:31–43. https://doi.org/10.1007/s10872-009-0003-2

Fukamachi Y, Mizuta G, Ohshima KI, Melling H, Fissel D, Wakatsuchi M (2003) Variability of sea-ice draft off Hokkaido in the sea of Okhotsk revealed by a moored ice-profiling sonar in winter of 1999. Geophys Res Lett 30:1376. https://doi.org/10.1029/2002GL016197

Fukamachi Y, Mizuta G, Ohshima KI, Toyota T, Kimura N, Wakatsuchi M (2006) Sea ice thickness in the Southwestern sea of Okhotsk revealed by a moored ice-profiling sonar. J Geophys Res 111:C09018. https://doi.org/10.1029/2005JC003327

Fukamachi Y, Tanaka I, Ohshima KI, Ebuchi N, Mizuta G, Yoshida H, Takayanagi S, Wakatsuchi M (2008) Volume transport of the Soya warm current revealed by bottom-mounted ADCP and ocean-radar measurement. J Oceanogr 64:385–392. https://doi.org/10.1007/s10872-008-0031-3

Fukamachi Y, Ohshima KI, Ebuchi N, Bando T, Ono K, Sano M (2010) Volume transport in the Soya Strait during 2006–2008. J Oceanogr 66:685–696. https://doi.org/10.1007/s10872-010-0056-2

Furuichi N, Higashi H, Sugimatsu K, Ohmura Y, Koshikawa H, Hasegawa T, Yamada H, Nambu R, Kaeriyama H (2019) Behavior of suspended particulate matter near the ocean bottom boundary layer. Bull Coast Oceanogr 57:21–30 (in Japanese)

Hanawa K, Mitsudera H (1985) On the data processings of daily mean values of oceanographical data: note on the daily mean sea-level data. Bull Coast Oceanogr 23:79–87 (in Japanese)

Huthnance JM (1978) On coastal trapped waves: analysis and numerical calculation by inverse iteration. J Phys Oceanogr 8:74–92. https://doi.org/10.1175/1520-0485(1978)008%3C0074:OCTWAA%3E2.0.CO;2

Imai M, Murayama A, Ono K, Yamashita Y, Suzuki K, Nakamaura T, Ohshima KI, Mitsudera H, Nishioka J (2024) Iron Supply Processes in the Southern Sea of Okhotsk. Proceedings of the 38th International Symposium on the Okhotsk Sea & Polar Oceans

Inoue R, Kitamura M, Fujiki T (2016) Diel vertical migration of zooplankton at the S1 biogeochemical mooring revealed from acoustic backscattering strength. J Geophys Res Oceans 121:1031–1050. https://doi.org/10.1002/2015JC011352

Ishizu M, Kitade Y, Matsuyama M (2006) Formation mechanism of the cold-water belt formed off the Soya warm current. J Oceanogr 62:457–471. https://doi.org/10.1007/s10872-006-0068-0

Ito M, Ohshima KI, Fukamachi Y, Mizuta G, Kusumoto Y, Nishioka J (2017) Observations of Frazil ice formation and upward sediment transport in the sea of okhotsk: A possible mechanism of iron supply to sea ice. J Geophys Res Oceans 122:788–802. https://doi.org/10.1002/2016JC012198

Ito M, Ohshima KI, Fukamachi Y, Hirano D, Mahoney AR, Jones J, Takatsuka T, Eicken H (2019) Favorable conditions for suspension freezing in an Arctic coastal polynya. J Geophys Res Oceans 124:8701–8719. https://doi.org/10.1029/2019JC015536

Ito M, Fukamachi Y, Ohshima KI, Shirasawa K (2020) Observational evidence of supercooling and Frazil ice formation throughout the water column in a coastal polynya in the sea of Okhotsk. Cont Shelf Res 196:104072. https://doi.org/10.1016/j.csr.2020.104072

Ito M, Ohshima KI, Fukamachi Y, Mizuta G, Kusumoto Y, Kikuchi T (2021) Underwater Frazil ice and its suspension depth detected from ADCP backscatter data around sea ice edge in the sea of Okhotsk. Cold Reg Sci Technol 192:103382. https://doi.org/10.1016/j.coldregions.2021.103382

Itoh M, Ohshima KI, Wakatsuchi M (2003) Distribution and formation of Okhotsk sea intermediate water: an analysis of isopycnal Climatological data. J Geophys Res 108:3258. https://doi.org/10.1029/2002JC001590

Iwagaki Y (1956) Hydrodynamical study on critical tractive force. J Jpn Soc Civ Eng 41:1–21

Kanna N, Toyota T, Nishioka J (2014) Iron and macro-nutrient concentrations in sea ice and their impact on the nutritional status of surface waters in the Southern Okhotsk sea. Prog Oceanogr 126:44–57. https://doi.org/10.1016/j.pocean.2014.04.012

Kanna N, Sibano Y, Toyota T, Nishioka J (2018) Winter iron supply processes fueling spring phytoplankton growth in a sub-polar marginal sea, the sea of okhotsk: importance of sea ice and the East Sakhalin current. Mar Chem 206:109–120. https://doi.org/10.1016/j.marchem.2018.08.006

Karaki T, Mitsudera H, Kuroda H (2018) Buoyancy shutdown process for the development of the baroclinic jet structure of the Soya warm current during summer. J Oceanogr 74:339–350. https://doi.org/10.1007/s10872-018-0465-1

Kishi S, Ohshima KI, Nishioka J, Isshiki N, Nihashi S, Riser SC (2021) The prominent spring bloom and its relation to sea-ice melt in the sea of Okhotsk, revealed by profiling floats. Geophys Res Lett 48:e2020GL091394. https://doi.org/10.1029/2020GL091394

Kuga M, Ohshima KI, Kimura N, Nakata K, Fukamachi Y (2023) Particle-tracking experiments of coastal-origin sea ice that could induce high biological productivity in the sea of Okhotsk. J Oceanogr 79:145–159. https://doi.org/10.1007/s10872-022-00670-5

Kuga M, Ohshima KI, Kishi S, Kimura N, Toyota T, Nishioka J (2024) Backward-tracking simulations of sea ice in the sea of Okhotsk toward Understanding of material transport through sea ice. J Oceanogr 80:59–70. https://doi.org/10.1007/s10872-023-00706-4

Liu Y, Guo J, Xue Y, Sangmanee C, Wang H, Zhao C, Khokiattiwong S, Yu W (2022) Seasonal variation in diel vertical migration of zooplankton and micronekton in the Andaman sea observed by a moored ADCP. Deep-Sea Res I 179:103663. https://doi.org/10.1016/j.dsr.2021.103663

Masunaga E, Yamazaki H (2014) A new tow-yo instrument to observe high-resolution coastal phenomena. J Mar Syst 129:425–436. https://doi.org/10.1016/j.jmarsys.2013.09.005

Mensah V, Ohshima KI, Drucker R, Riser S (2024) Evaluation of the water mass composition in the sea of Okhotsk and its long-term change using an advanced mapping technique. J Geophys Res 129:e2023JC020374. https://doi.org/10.1029/2023JC020374

Mizuta G, Ohshima KI, Fukamachi Y, Wakatsuchi M (2005) The variability of the East Sakhalin current induced by winds over the continental shelf and slope. J Mar Res 63:1017–1039

Nakatsuka T, Toda M, Kawamura K, Wakatsuchi M (2004) Dissolved and particulate organic carbon in the sea of okhotsk: transport from continental shelf to ocean interior. J Geophys Res Oceans 109. https://doi.org/10.1029/2003JC001909. C09S14

Nishioka J, Ono, Saito, Sakaoka K, Yoshimura T (2011) Oceanic iron supply mechanisms which support the spring diatom bloom in the Oyashio region, Western Subarctic Pacific. J Geophys Res Oceans 116:C02021. https://doi.org/10.1029/2010JC006321

Nishioka J, Nakatsuka T, Watanabe YW, Yasuda I, Kuma K, Ogawa H, Ebuchi N, Scherbinin A, Volkov YN, Shiraiwa T, Wakatsuchi M (2013) Intensive mixing along an Island chain controls oceanic biogeochemical cycles. Global Biogeochem Cycles 27:920–929. https://doi.org/10.1002/gbc.20088

Nishioka J, Nakatsuka T, Ono K, Volkov YN, Scherbinin A, Shiraiwa T (2014) Quantitative evaluation of iron transport processes in the sea of Okhotsk. Prog Oceanogr 126:180–193. https://doi.org/10.1016/j.pocean.2014.04.011

Nishioka J, Obata H, Hirawake T, Kondo Y, Yamashita Y, Misumi KYasuda I (2021) A review: iron and nutrient supply in the Subarctic

Pacific and its impact on phytoplankton production. J Oceanogr 77:561–587. https://doi.org/10.1007/s10872-021-00606-5
Ohshima KI (1986) Frontal waves and vertical circulation on the Soya warm current. Otsuchi Mar Res Cent Rep 12:56–57 (in Japanese)
Ohshima KI (1994) The flow system in the Japan sea caused by a sea level difference through shallow Straits. J Geophys Res Oceans 99:9925–9940. https://doi.org/10.1029/94JC00170
Ohshima KI, Simizu D (2008) Particle tracking experiments on a model of the Okhotsk sea: toward oil spill simulation. J Oceanogr 64:103–114. https://doi.org/10.1007/s10872-008-0008-2
Ohshima KI, Simizu D, Ebuchi N, Morishima S, Kashiwase H (2017) Volume, heat, and salt transports through the Soya Strait and their seasonal and interannual variations. J Phys Oceanogr 47:999–1019. https://doi.org/10.1175/JPO-D-16-0210.1
Rubey WW (1933) Settling velocity of gravel, sand, and silt particles. Am J Sci Ser 5:325–338
Tanabe T, Sakamoto T (2002) The grain and mineral analysis of sea-floor sediment and its origin in the Southwestern Okhotsk sea collected by the GH00 and GH01 cruises. GSJ Interim Rep 25:73–98 (in Japanese)
Wadaka M, Matsuyama M, Ishizu M, Kitade Y, Yano Y (2009) Bottom high turbidity water observed off the Soya warm current. Bull Coast Oceanogr 46:175–183 (in Japanese)
Watanabe T, Wakatsuchi M (1998) Formation of 26.8–26.9 σ_θ water in the Kuril basin of the sea of Okhotsk as a possible origin of North Pacific intermediate water. J Geophys Res Oceans 103:2849–2865. https://doi.org/10.1029/97JC02914